FRONTIERS OF PHYSICS

RESEARCH ARTICLE
Volume 21 / Issue 12 / 125201 / 2026

Gate-tunable phosphorene-topological insulator based spin transistor

Yue-Heng Liu[1,2,3], Ruigang Li[1,2,3,†], Jun-Feng Liu[1,‡]

1 School of Physics and Materials Science, Guangzhou University, Guangzhou 510006, China
2 GBA Branch of Aerospace Information Research Institute, Chinese Academy of Sciences, Guangzhou 510700, China
3 Guangdong Provincial Key Laboratory of Terahertz Quantum Electromagnetics, Guangzhou 510700, China
Corresponding authors. E-mail: †liruigang@gzhu.edu.cn, ‡phjfliu@gzhu.edu.cn
Received October 1, 2025; accepted January 26, 2026

ABSTRACT

We investigated the gate-tunable spin transistor structured as a ferromagnet–topological insulator–ferromagnet junction implemented on a zigzag phosphorene nanoribbon. By applying a gate voltage to the device region, the wave vector of the channel can be effectively modulated, thereby shifting the resonance condition of the junction and enabling efficient tuning of the spin-dependent conductance. The conductance of the junction can be switched between e^2/h and 0, corresponding to the ON and OFF states, respectively. Our work demonstrates a feasible strategy for realizing spin transistors and highlights the potential of such systems for future spintronic applications.

Keywords phosphorene nanoribbon, gate-tunable spin transistor, quantum transport

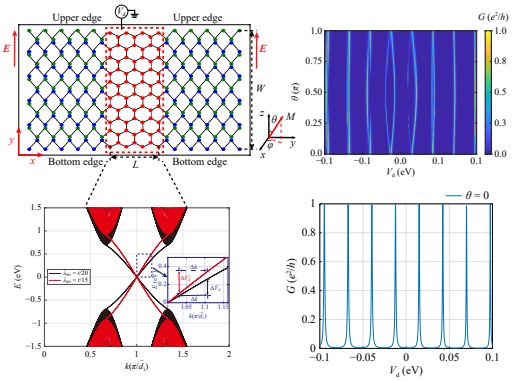

1 Introduction

The Datta–Das spin field-effect transistor (spin-FET) [1–4] has long been regarded as a promising candidate for future spintronic devices [5–10]. Its gate-tunable characteristics — particularly the ability to electrically control spin transport — represent a significant advantage in modern electronic applications, aligning with the ongoing pursuit of nonvolatile, low-power, and high-speed logic and memory technologies. However, the experimental realization of such a device remains challenging due to four critical requirements: (i) long spin relaxation times (or spin diffusion lengths), (ii) high-efficiency spin injection at the ferromagnet/semiconductor interface, (iii) confinement to a ballistic quasi-one-dimensional (quasi-1D) transport channel, and (iv) effective gate modulation of spin precession via SOI. A viable strategy for constructing gate-tunable spin transistors is highly demanded.

Phosphorene, a two-dimensional single-elemental material, exhibits exceptional promise for spintronic applications due to its intrinsically long spin relaxation time/length and high spin injection efficiency [11–17]. Notably, as demonstrated in Ref. [11], phosphorene can achieve remarkable spin relaxation lengths exceeding 6 μm at room temperature. Both theoretical and experimental studies have revealed that edge magnetism can be systematically induced in phosphorene nanoribbons: charge doping has been shown to induce magnetic ordering in armchair phosphorene nanoribbons (APNRs) [12], while oxygen-passivated tilted phosphorene nanoribbons exhibit an edge-to-edge antiferromagnetic ground state [13]. Similar magnetic phenomena have been observed in zigzag phosphorene nanoribbons (ZPNRs), though the edge magnetism vanishes when edge dangling bonds are passivated or when the ribbon width exceeds 3 nm [16].

Higher Education Press

https://doi.org/10.15302/frontphys.2026.125201

Importantly, this limitation can be overcome by depositing phosphorene on an EuO substrate, leveraging the proximity effect to induce emergent magnetic properties [17]. These controllable magnetic properties, coupled with phosphorene's superior spin transport characteristics, underscore its significant potential for the development of advanced spintronic devices [18, 19].

Moreover, the edge states of ZPNRs form quasi-1D conducting channels, a key feature enabling the realization of a spin transistor, which can be efficiently modulated by an external electric field. Importantly, the edge bands are entirely decoupled from the bulk bands, effectively eliminating interference from bulk states and significantly enhancing spin transport controllability [20]. This decoupling offers a distinct advantage for optimizing the performance of spin transitors.

In recent years, topological insulators (TIs) have emerged as a promising candidate for next-generation electronics, demonstrating rapid experimental and theoretical progress [21–23]. TIs are characterized by host nontrivial topological surface states originating from their bulk band topology. Typically, these surface states exhibit spin polarization, with the spin-polarized channels possessing opposite chirality. Crucially, the transport properties of TI-based devices are dominated by these surface states, which can be effectively modulated via electrostatic gating, enabling precise electrical control over spin-dependent transport.

In this work, we systematically investigate the transport properties of a phosphorene-TI based spin transistor. The junction consists of a TI layer sandwiched between two ferromagnetic ZPNRs. Spin-polarized electrons are injected into the junction under an in-plane electric field applied across the ZPNRs. By modulating the gate voltage in the TI region, the conductance of the junction can be effectively controlled, enabling distinct ON and OFF states, corresponding to the conductance e^2/h and 0 respectively. Different from junctions constructed solely on TIs, the interplay between topologically trivial and nontrivial edge states can give rise to interference at the phosphorene-TI interface, resulting in pronounced conductance oscillations. Our study presents a simple, practical, and promising strategy for designing efficient spin transistors.

2 Structure and model

The junction under investigation is schematically depicted in Fig. 1(a). Without loss of generality, the device incorporates a honeycomb-lattice TI model. Figure 1(c) shows the primitive cell of the TI-based device, which has dimensions of $L \times W = N_L\tilde{d}_1 \times N_W\tilde{d}_2$, where N_L and N_W denote the number of unit cells along the x and y directions, respectively. $\tilde{d}_1 = 0.246$ nm and $\tilde{d}_2 = 0.426$ nm represent the lengths of the lattice vector

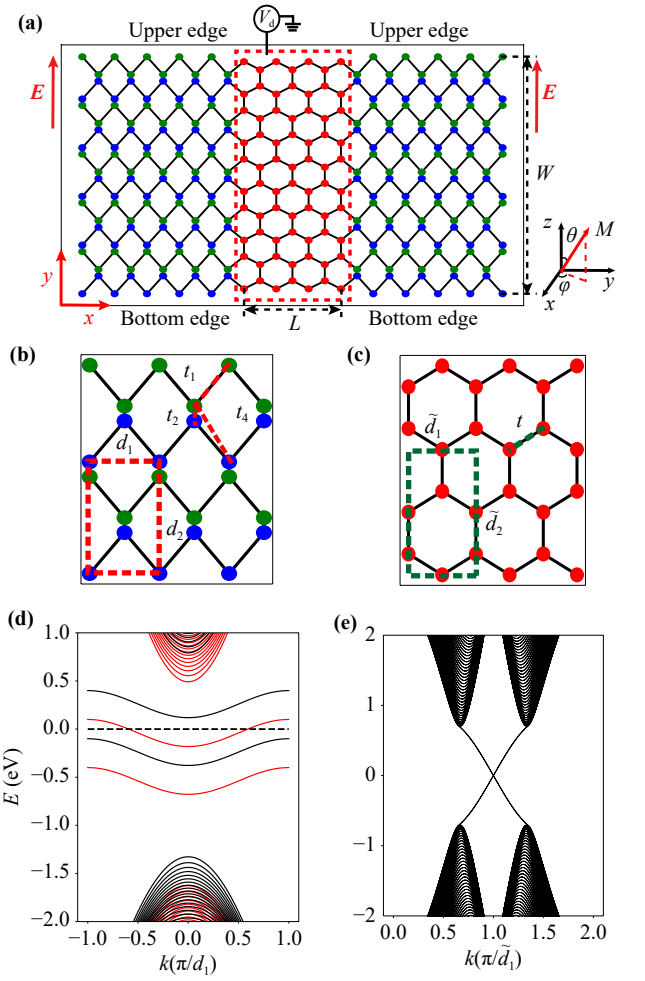

Fig. 1 Schematics of **(a)** the phosphorene-topological insulator-phosphorene junction. **(b)** the ZPNR and **(c)** the honeycomb-lattice TI model. Band structures of **(d)** the ZPNR and **(e)** the honeycomb-lattice TI model. Note that the red and black lines in Fig. (d) denote the spin-up and spin-down bands, respectively.

of the TI region.

The primitive cell of the zigzag phosphorene nanoribbon (ZPNR) is illustrated in Fig. 1(b), with the lengths of lattice vector $d_1 = 0.327$ nm and $d_2 = 0.443$ nm [24], respectively. In-plane electric fields are applied to the leads, while an gate voltage is introduced in the device region. Additionally, magnetization is induced in the ZPNR leads by coupling them to EuO substrates, with the exchange energy $M \approx 0.15$ eV [17]. Note that the EuO substrate provides a strong exchange field to the phosphorene, which effectively suppresses the effect of SOI on the conductance of the junction. In this configuration, the magnetization direction forms an angle θ with respect to the z-direction — which, by default, is aligned parallel to the spin polarization direction of the TI channel. Without losing generality, the direction of magnetization of left and right lead is set as the same, i.e., $\theta_{\rm L} = \theta_{\rm R} = \theta$.

The Hamiltonian of the system can be written as

$$H = H_C + H_{\rm L} + H_{\rm R} + H_{cp}, \tag{1}$$

where H_C and $H_{\rm L/R}$ represent the Hamiltonian for the TI and the left/right lead, respectively, where

$$\begin{aligned} H_C =& \sum_{i\in C} V_d a_i^\dagger \sigma_0 a_i - t \sum_{\langle i,j\rangle\in C} (a_i^\dagger \sigma_0 a_j + h.c.) \\ & - \sum_{\langle\langle i,j\rangle\rangle\in C} (\mathrm{i}\lambda_{SO} v_{ij} a_i^\dagger \sigma_z a_j + h.c.), \\ H_{\rm L/R} =& \sum_{i\in {\rm L/R}} a_i^\dagger \Big(\boldsymbol{\sigma}\cdot \boldsymbol{M}_{\rm L/R} + \eta\Big(\frac{y}{W} - \frac{1}{2}\Big) E_y \sigma_0\Big) a_i \\ & - \sum_{i,j\in {\rm L/R}} (t_{ij} a_i^\dagger \sigma_0 a_j + h.c.). \end{aligned} \tag{2}$$

$\boldsymbol{\sigma}$ and $\boldsymbol{\sigma_0}$ denote the Pauli matrix and identity matrix, respectively. $a_{is}^\dagger/a_{is}$ is the create/annihilate operator with spin $s =\uparrow,\downarrow$ on site i. In H_C, the parameter t represents the nearest-neighbor (denoted as $\langle i,j\rangle$) hopping integral in the scattering region, where $t = -2.7$ eV. V_d denotes the gate voltage. The SOI is introduced between next-nearest-neighbor (denoted as $\langle\langle i,j\rangle\rangle$) sites with a strength of $\lambda_{SO} = 0.05t$ [25]. Here, $v_{ij} = 1$ if an electron moves counterclockwise from site j to site i, and $v_{ij} = -1$ otherwise [26].

In the first term of $H_{\rm L/R}$, $\boldsymbol{M}_{\rm L}$ and $\boldsymbol{M}_{\rm R}$ represent the magnetizations of the left and right leads, respectively, and $|E_y|/2$ corresponds to the maximum on-site energy induced by the in-plane electric field, which is aligned with y-direction [Fig. 1(a)]. The second term describes nearest-neighbor hopping with the hopping integrals t_{ij}, where $t_1 = -1.220$ eV, $t_2 = 3.665$ eV, $t_3 = -0.205$ eV, $t_4 = -0.105$ eV, $t_5 = 0.055$ eV [27], as shown in Fig. 1(b). According to Ref. [19], the hopping t_3 and t_5 can be neglected since they have a negligible effect on the electronic properties of phosphorene nanoribbons.

The coupling between the TI region and the phosphorene leads is described by

$$H_{cp} = - \sum_{i\in C, j\in {\rm L/R}} (t_c a_i^\dagger \sigma_0 a_j + h.c.). \tag{3}$$

The hopping integrals is set as $t_c = -0.5$ eV. Note that the spin orientation of the topological insulator's transport channels is conventionally defined along the z-direction. When spin-polarized electrons are injected at an angle θ to the transport channel of a TI, a unitary transformation in the phosphorene lead $\tilde{a}_i = U a_i$ can be applied, where

$$U = \begin{pmatrix} \cos(\theta/2) & \mathrm{e}^{-\mathrm{i}\varphi}\sin(\theta/2) \\ \mathrm{e}^{\mathrm{i}\varphi}\sin(\theta/2) & \cos(\theta/2) \end{pmatrix}, \tag{4}$$

where φ represents the azimuth angle of the magnetization with respect to the x-direction, as shown in Fig. 1(a). The magnetization $\boldsymbol{M}_{\rm L/R}$ can be written as $\boldsymbol{M}_{\rm L/R} = M(\sin\theta\cos\varphi, \sin\theta\sin\varphi, \cos\theta)$, where M is the modulus of the magnetization. After the transformation, the Hamitonian $H_{\rm L/R}$ become

$$\begin{aligned} H_{\rm L/R} =& \sum_{i\in {\rm L/R}} \tilde{a}_i^\dagger \Big[\boldsymbol{\sigma}\cdot\tilde{\boldsymbol{M}}_{\rm L/R} + \Big(\frac{y}{W} - \frac{1}{2}\Big) E_y \sigma_0\Big] \tilde{a}_i \\ & - \sum_{i,j\in {\rm L/R}} (t_{ij} \tilde{a}_i^\dagger \sigma_0 \tilde{a}_j + h.c.), \\ H_{cp} =& - \sum_{\langle i,j\rangle} (t_c a_i^\dagger \sigma_0 U^\dagger \tilde{a}_j + h.c.), \end{aligned} \tag{5}$$

where $\tilde{\boldsymbol{M}}_{\rm L/R} = U\boldsymbol{M}_{\rm L/R}U^\dagger$. According to the Landauer–Büttiker formula [28], the conductance can be given as

$$G(E_F) = \frac{e^2}{h} {\rm Tr}[\Gamma_{\rm R}(E_F) G^R(E_F) \Gamma_{\rm L}(E_F) G^A(E_F)], \tag{6}$$

where the line-width function $\Gamma_{\rm L/R} = \mathrm{i}[\sum_{\rm L/R}^R - \sum_{\rm L/R}^A]$. $\sum_{\rm L/R}^{R/A}$ is the retarded/advanced self-energy function coupling to the left/right lead, which can be calculated numerically by solving the surface Green's function of the left/right lead [29, 30]. The retarded Green's function is $G^R = [G^A]^\dagger = 1/(E_F - H_C - \sum_{\rm L}^R - \sum_{\rm R}^R)$.

To investigate the transport properties, we computed the Green's function of the structure using the Python package Kwant [31]. This package enables the construction of a tight-binding model based on system parameters such as the lattice structure and device geometry. From this model, the Green's function and the corresponding wave functions of scattered states can be directly obtained using the built-in functionality of Kwant.

3 Result and discussion

The band structures of the ZPNR and honeycomb-lattice TI nanoribbon are shown in Figs. 1(d) and (e), respectively. Without magnetizations $\boldsymbol{M}_{\rm L/R}$ and electric fields E_y, four degenerate edge bands appear within the band gap of the bare ZPNR. The magnetization $M = -0.15$ eV splits these degenerate states into two double-degenerate bands. When an in-plane electric field is applied along the $+y$ direction, an additional potential $E_y = 0.5$ eV between the edges: electrons at the bottom edge acquire a potential of –0.25 eV, while those at the upper edge gain +0.25 eV. This is implemented via the electric field term in the on-site potential of the Hamiltonian $H_{\rm L/R}$. As a result, the four initially degenerate states separate as shown in Fig. 1(d). Without loss of generality, we call the red and black solid lines denote the spin-up and spin-down states, respectively. Due to the narrow bandwidth of the edge states, each split band can individually inject spin-polarized electrons into the system when the Fermi energy is set to the required value. Figure 1(e) displays the band structure of the TI ribbon with $N_W = 70$, and the bulk band gap is given by

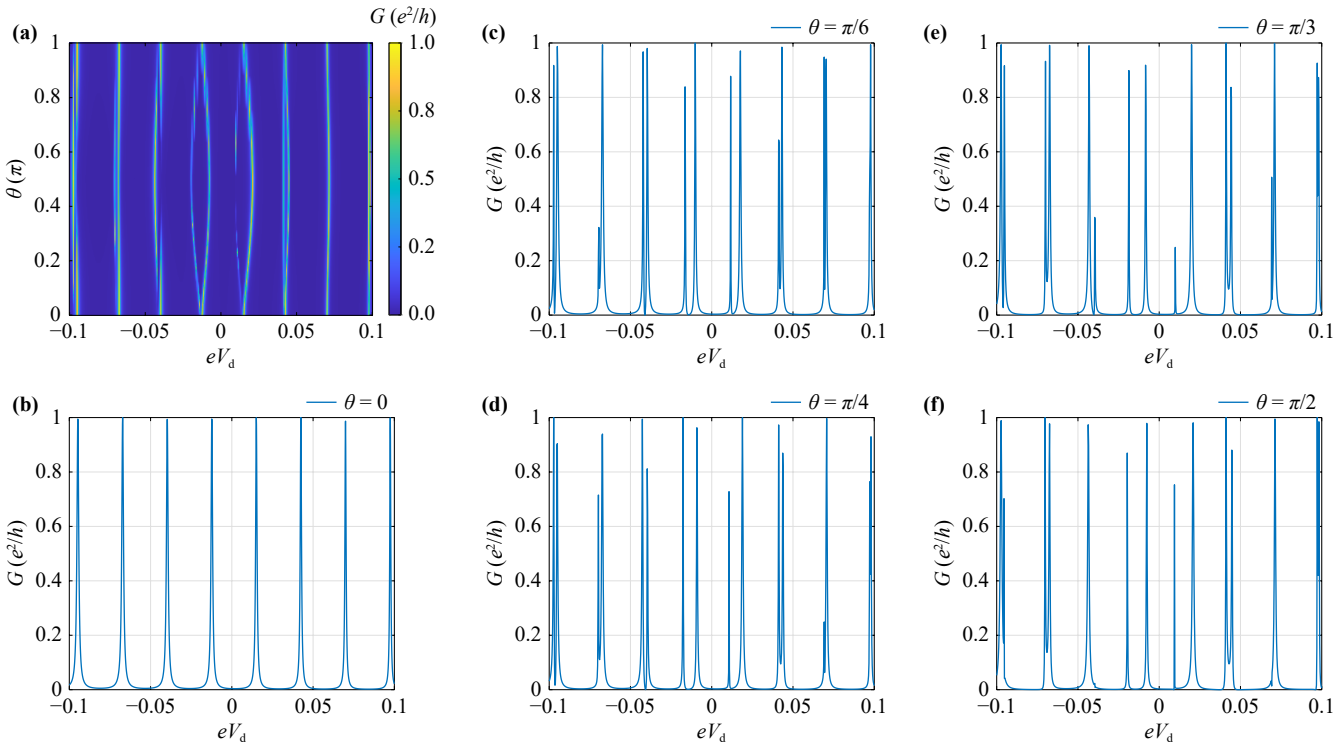

Fig. 2 **(a)** The conductance as a function of gate voltage V_d and magnetization angle θ, with the size of devic $N_W = 70$ and $N_L = 40$. Specifically, the conductance versus energy V_d is plotted for several representative magnetization angles: **(b)** $\theta = 0$, **(c)** $\theta = \pi/6$, **(d)** $\theta = \pi/4$, **(e)** $\theta = \pi/3$, and **(f)** $\theta = \pi/2$.

$\delta = 2\lambda_{SO}$. Two spin-polarized chiral edge states are localized within the gap. For clarity, we denote the channel with spin parallel/antiparallel to the z-direction as the $\langle +z\rangle$ / $\langle -z\rangle$ channel.

The Fermi energy is set to be 0 eV, enabling the individual injection of spin-up electrons from upper edge. As the spin-up states are oriented at an angle θ relative to the z-direction, the hopping integral between spin-up electron and the $\langle +z\rangle$ channel is given by $t_c \cos(\theta/2)$, where the cosine term corresponds to the matrix element U_{11} of the unitary transformation U. Meanwhile, the hopping integral between the spin-up electrons and $\langle -z\rangle$ channel is described by U_{12}, specifically $t_c e^{-i\varphi} \sin(\theta/2)$. Therefore, by adjusting the magnetization angle θ, spin-up electrons from the leads can hop into the both spin-polarized channels, which is possible to control the available transport channels for electrons within the scattering region. Furthermore, an additional gate voltage V_d is added to the TI region, causing a shift in its on-site energy, i.e., $\varepsilon_C + V_d$.

The junction conductance is numerically investigated as a function of the angle θ and the gate voltage V_d, as illustrated in Fig. 2. It is easy to find that, the conductance remains invariant under complementary magnetization angles, i.e., $G(\theta) = G(\pi - \theta)$, a symmetry that can be accounted for by Eq. (5). Spin-up electrons injected from the lead couple effectively to the $\langle +z\rangle$ and $\langle -z\rangle$ channels within the scattering region, mediated by the hopping strengths $U_{11}(\theta)$ and $U_{12}(\theta)$, respectively. It is noteworthy that the relations $U_{11}(\pi - \theta) = U_{12}(\theta)$ and $U_{12}(\pi - \theta) = U_{11}(\theta)$ hold, which directly leads to the symmetry $G(\theta) = G(\pi - \theta)$. It should be noted that the junction conductance is independent of the azimuth angle φ, as the phase induced by φ cancels out during the transport process.

When θ is fixed, the conductance can be effectively modulated by V_d, since the gate voltage influences the wave vector of the transport states in the channel, thereby altering the resonance condition given by $2k(L + W) = n\pi$. The wave vector depends on V_d as $k = \chi V_d$, where χ is a conversion coefficient determined by the spin–orbit coupling strength λ_{SO}, approximately given by $\chi \approx \lambda_{SO}/[\pi/(3d_1)]$. The corresponding period of oscillation in conductance is $\Delta k = \chi \Delta V_d = \pi/[2(L + W)]$. Thus, once the device dimensions and λ_{SO} are fixed, the conductance can be directly and efficiently controlled by the gate voltage V_d.

When the angle θ is set to 0 — that is, the magnetization is aligned along the z-axis — the conductance exhibits perfect periodicity as a function of the gate voltage V_d, as shown in Fig. 2(b). This behavior can be understood that when an electron injected into the junction along upper edge enters the $\langle +z\rangle$ channel, it propagates along the edges of the TI and interferes with itself, resulting in

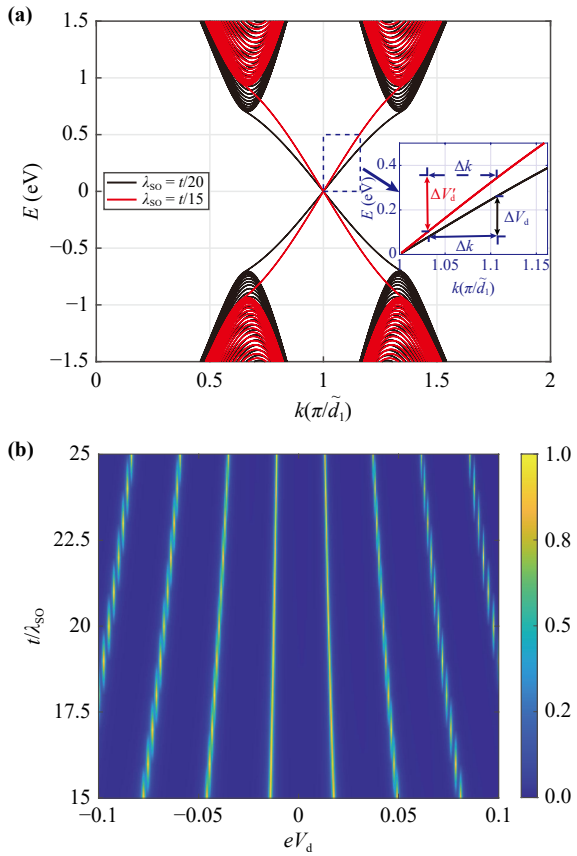

Fig. 3 **(a)** The band of TI with different SOI. **(b)** The conductance as a function of the gate voltage V_d and the strength of SOI λ_{SO}, with the size of device $N_W = 70$ and $N_L = 40$.

conductance oscillations. The junction conductance oscillates between e^2/h (ON state) and 0 (OFF state), with a period of approximately 27 meV as observed in Fig. 2. We also present the system conductance as a function of energy V for $\theta = \pi/6$, $\pi/4$, $\pi/3$, and $\pi/2$ in Figs. 2(c), (d), (e), (f), respectively. It can be confirmed that the center positions of the resonance peaks remain unchanged at any angle θ. As the magnetization angle θ deviates from the z-axis (i.e., $\theta \neq 0$), the perfect periodicity of the conductance is gradually disrupted, manifesting as a splitting of the resonance peaks. We found that, as shown in Fig. 2(a), the conductance peak near $V_d = 0$ eV exhibits clear splitting into two distinct peaks, particularly at $\theta = \pi/2$. This splitting arises from multiple interference effects due to spin-up electrons hopping into two distinct channels.

The strength of SOI in the TI device primarily influences the slope of the edge states. As the strength of SOI increases, the bulk gap increases, with the positions of the valleys in k-space remain unchanged. Correspondingly, the slope of the edge states connecting the two valleys increases, shown in Fig. 3(a). The increasing slope of the edge state correspond to an increase in the oscillation period of the conductance as a function of V_d, as illustrated in Fig. 3(b).

When the electric fields in the left and right leads change from parallel to antiparallel alignment, the corresponding band structures are shown in Fig. 4(a). The results indicate that the band structures of the left and right leads remain identical, except that the spin states propagate in opposite edges when $E_F = 0$. For instance, at $E_F = 0$, when an electric field is applied parallel to the left lead, electrons are emitted from the upper edge of the right lead. Conversely, when the electric field of the right lead is reversed, electrons are emitted from the bottom edge. The density of states corresponding to these two scenarios is shown in Figs. 4(b) and (c), respectively. It means that, reversing the in-plane electric field does not change the spin polarization of the

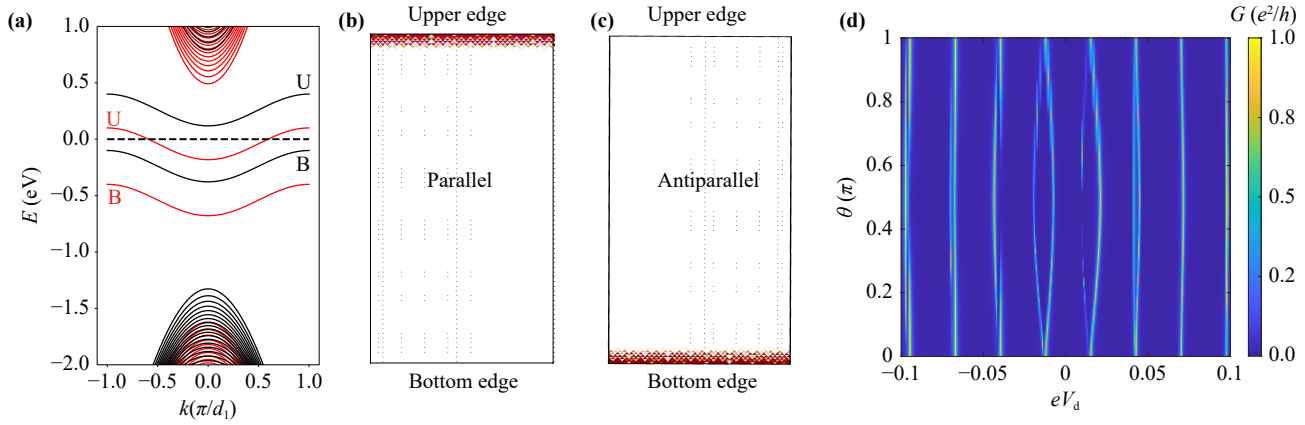

Fig. 4 **(a)** Band structure and local density of states of the right lead under an in-plane electric field applied **(b)** parallel or **(c)** antiparallel to the left lead, where the red and black symbol "U" and "B" in subfigure (a) denote the upper and bottom edges displayed in panel (b), respectively. **(d)** Conductance as a function of gate voltage V_d and magnetization angle θ, with the in-plane electric field applied to the right lead in the antiparallel direction relative to the left lead. The size of device $N_W = 70$ and $N_L = 40$.

injected electrons, but causes the injection edge to shift from the upper to the bottom edge, as illustrated by the local density of states of electrons in the left and right leads in Figs. 4(b, c). The conductance as a function of θ and V_d, shown in Fig. 4(d), is exactly the same as that in Fig. 2(a). This clearly demonstrates that the conductance remains unaffected when the in-plane electric fields in the left and right leads switch from parallel to antiparallel alignment. These findings confirm that first-order interference occurs with a path difference of $2k(L+W)$ in both cases.

Figure 4(d) shows the conductance variation with the angle θ and energy V in this case. We found that when the electric field is set in the opposite direction, the numerical results exhibit all the characteristic changes observed in Fig. 2(a), and the corresponding conductance values are approximately the same.

4 Conclusion

In this work, we propose an electrically controllable spin transistor based on a zigzag phosphorene nanoribbon (ZPNR). Spin-polarized electrons are injected from the ferromagnetic ZPNR electrode, modulated within the topological insulator (TI) channel, and subsequently ejected from the junction. The resonant condition in the channel can be effectively tuned by a gate voltage, resulting in conductance oscillations that define the ON and OFF states of the device. Our findings offer a practical strategy for designing tunable spintronic devices.

Declarations The authors declare that they have no competing interests and there are no conflicts.

Acknowledgements This project was supported by the National Natural Science Foundation of China (Grant Nos. 62588201 and 12174077) and Guangdong Basic and Applied Basic Research Foundation (Grant No. 2022A1515110011).

References

1. M. Ciorga, Perspective on the spin field-effect transistor, *J. Phys. D Appl. Phys.* 58, 012001 (2024)
2. G. F. A. Malik, M. A. Kharadi, F. A. Khanday, and N. Parveen, Spin field effect transistors and their applications: A survey, *Microelectronics J.* 106, 104924 (2020)
3. Y. Semenov, K. Kim, and J. Zavada, Spin field effect transistor with a graphene channel, *Appl. Phys. Lett.* 91(15), 153105 (2007)
4. W. Yan, O. Txoperena, R. Llopis, H. Dery, L. E. Hueso, and F. Casanova, A two-dimensional spin field-effect switch, *Nat. Commun.* 7(1), 13372 (2016)
5. E. S. Grichuk and E. A. Manykin, Spin polarized quantum pump effect in zigzag graphene nanoribbons, *JETP Lett.* 93(7), 372 (2011)
6. Q. Zhang, K. S. Chan, and Z. Lin, Spin current generation by adiabatic pumping in monolayer graphene, *Appl. Phys. Lett.* 98(3), 032106 (2011)
7. D. Bercioux, D. F. Urban, F. Romeo, and R. Citro, Rashba spin–orbit-interaction-based quantum pump in graphene, *Appl. Phys. Lett.* 101(12), 122405 (2012)
8. P. Michetti, P. Recher, and G. Iannaccone, Electric field control of spin rotation in bilayer graphene, *Nano Lett.* 10(11), 4463 (2010)
9. P. Seneor, B. Dlubak, M. B. Martin, A. Anane, H. Jaffres, and A. Fert, Spintronics with graphene, *MRS Bull.* 37(12), 1245 (2012)
10. K. Vaklinova, A. Hoyer, M. Burghard, and K. Kern, Current-induced spin polarization in topological insulator –graphene heterostructures, *Nano Lett.* 16(4), 2595 (2016)
11. A. Avsar, J. Y. Tan, M. Kurpas, M. Gmitra, K. Watanabe, T. Taniguchi, J. Fabian, and B. Özyilmaz, Gate-tunable black phosphorus spin valve with nanosecond spin lifetimes, *Nat. Phys.* 13(9), 888 (2017)
12. M. U. Farooq, A. Hashmi, and J. Hong, Manipulation of magnetic state in armchair black phosphorene nanoribbon by charge doping, *ACS Appl. Mater. Interfaces* 7(26), 14423 (2015)
13. Y. Jing, X. Zhang, and Z. Zhou, Phosphorene: What can we know from computations? *Wiley Interdiscip. Rev. Comput. Mol. Sci.* 6(1), 5 (2016)
14. Z. Zhu, C. Li, W. Yu, D. Chang, Q. Sun, and Y. Jia, Magnetism of zigzag edge phosphorene nanoribbons, *Appl. Phys. Lett.* 105(11), 113105 (2014)
15. Y. Du, H. Liu, B. Xu, L. Sheng, J. Yin, C. G. Duan, and X. Wan, Unexpected magnetic semiconductor behavior in zigzag phosphorene nanoribbons driven by half-filled one dimensional band, *Sci. Rep.* 5(1), 8921 (2015)
16. M. Rahman, K. Zhou, Q. Xia, Y. Nie, and G. Guo, Spin-dependent transport properties of zigzag phosphorene nanoribbons with oxygen-saturated edges, *Phys. Chem. Chem. Phys.* 19(37), 25319 (2017)
17. H. Chen, B. Li, and J. Yang, Proximity effect induced spin injection in phosphorene on magnetic insulator, *ACS Appl. Mater. Interfaces* 9(44), 38999 (2017)
18. M. A. M Keshtan and M. Esmaeilzadeh, Spin filtering in a magnetized zigzag phosphorene nanoribbon, *J. Phys. D Appl. Phys.* 48(48), 485301 (2015)
19. R. Li, J. F. Liu, and J. Wang, Electrically controllable spin filtering in zigzag phosphorene nanoribbon based normal–antiferromagnet–normal junctions, *Chin. Phys. B* 33(1), 017304 (2023)
20. R. Li, L. Chen, J. F. Liu, and J. Wang, Crossed Andreev reflection in zigzag phosphorene nanoribbon based ferromagnet/superconductor/ferromagnet junctions, *Sci. Rep.* 12(1), 6079 (2022)
21. Y. Fan and K. L. Wang, Spintronics based on topological insulators, in: Spin, Vol. 6, World Scientific, 2016, p. 1640001
22. M. He, H. Sun, and Q. L. He, Topological insulator: Spintronics and quantum computations, *Front. Phys. (Beijing)* 14(4), 43401 (2019)
23. F. D. M. Haldane, Model for a quantum hall effect without landau levels: Condensed-matter realization of the "parity anomaly", *Phys. Rev. Lett.* 61(18), 2015

(1988)
24. A. Castellanos-Gomez, L. Vicarelli, E. Prada, J. O. Island, K. L. Narasimha-Acharya, S. I. Blanter, D. J. Groenendijk, M. Buscema, G. A. Steele, J. V. Alvarez, H. W. Zandbergen, J. J. Palacios, and H. S. J. van der Zant, Isolation and characterization of few-layer black phosphorus, *2D Mater.* 1, 025001 (2014)
25. Q. Zhang, K. Chan, and J. Li, Spin-transfer torque generated in graphene based topological insulator heterostructures, *Sci. Rep.* 8(1), 4343 (2018)
26. E. E. Colomés and M. Franz, Antichiral edge states in a modified Haldane nanoribbon, *Phys. Rev. Lett.* 120(8), 086603 (2018)
27. A. N. Rudenko and M. I. Katsnelson, Quasiparticle band structure and tight-binding model for single-and bilayer black phosphorus, *Phys. Rev. B* 89(20), 201408 (2014)
28. Y. Y. Meir and N. S. Wingreen, Landauer formula for the current through an interacting electron region, *Phys. Rev. Lett.* 68(16), 2512 (1992)
29. D. H. Lee and J. D. Joannopoulos, Simple scheme for surface-band calculations. ii. the green's function, *Phys. Rev. B* 23(10), 4997 (1981)
30. M. L. Sancho, J. L. Sancho, J. L. Sancho, and J. Rubio, Highly convergent schemes for the calculation of bulk and surface green functions, *J. Phys. F Met. Phys.* 15(4), 851 (1985)
31. C. W. Groth, M. Wimmer, A. R. Akhmerov, and X. Waintal, Kwant: A software package for quantum transport, *New J. Phys.* 16(6), 063065 (2014)